Scale Dependence of Effective Hydraulic Conductivity Distributions in 3D Heterogeneous Media: A Numerical Study

A. Boschan & B. Nœtinger

Transport in Porous Media

ISSN 0169-3913

Transp Porous Med
DOI 10.1007/s11242-012-9991-2

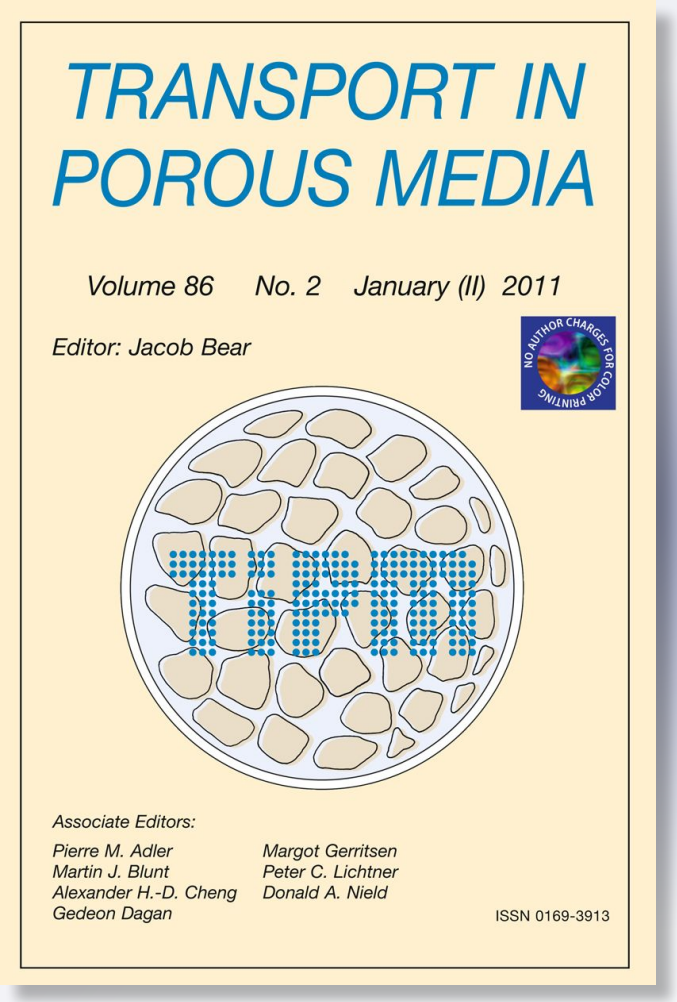

Springer

Transp Porous Med
DOI 10.1007/s11242-012-9991-2

Scale Dependence of Effective Hydraulic Conductivity Distributions in 3D Heterogeneous Media: A Numerical Study

A. Boschan · B. Nœtinger

Received: 16 December 2011 / Accepted: 13 March 2012

Abstract Upscaling procedures and determination of effective properties are of major importance for the description of flow in heterogeneous porous media. In this context, we study the statistical properties of effective hydraulic conductivity (K_{eff}) distributions and their dependence on the coarsening scale. First, we focus on lognormal stationary isotropic media. Our results suggest that K_{eff} is lognormally distributed independently on the coarsening scale. The scale dependence of the mean and variance of K_{eff} are in agreement with recent analytical derivations obtained using coarse graining filtering techniques. In the second part, we focus on binary media, analysing the dependence of K_{eff} distributions on the coarsening scale and also on the high-K facies volume fraction p. When p is near the percolation threshold p_c, the decrease of the normalized variance with the coarsening scale is remarkably (10^2 times) slower compared to the situation in which p far from p_c, but also compared to the cases of lognormal media studied before. This result permits to assess the degree of difficulty that systems with p near p_c pose for upscaling procedures. Also we point out in terms of K_{eff} statistics the relative influence of the coarsening scale and of the high-K facies connectivity.

Keywords Heterogeneity · Upscaling · Random media · Effective conductivity · Single phase flow

1 Introduction

1.1 Upscaling

Typical geological description of the subsurface heterogeneity involves spatial scales ranging from microns (typical pore size, attainable using thin sections observations, or NMR

A. Boschan (✉) · B. Nœtinger
IFP Energies Nouvelles, Rueil Malmaison, France
e-mail: aboschfi@gmail.com

Present Address:
A. Boschan
Grupo de Medios Porosos, CONICET, CABA, Paseo Colón 850, Buenos Aires, Argentina

Published online: 05 April 2012

techniques) to several kilometres (typical reservoir scale, attainable with 3D seismics, outcrops and geological analysis). Basic laboratory measurements are usually performed at the centimetre scale corresponding to the plug size. Geological data can be determined at the scale of m in the direction of the wells or boreholes, using well logging tools.

In most cases, simulating flow and transport models at the finest resolution scale remains computationally expensive. Even if fine grid simulations could be performed for several reservoir realizations, practical applications such as history matching, uncertainty modelling and sensitivity analysis would still remain unfeasible at this scale. Upscaling procedures and techniques are then of interest to transfer data from the fine geological grid to the coarse simulation one. The issue of upscaling in heterogeneous media was initially addressed a few decades ago by Landau and Lifshitz (1960) in the context of electrodynamics and by Matheron (1967) in the context of porous media. Analytical methods like bounds-based approaches (Renard and de Marsily 1997) or power averaging (Journel et al. 1986; Desbarats 1992) were initially proposed, before using numerical techniques related to homogenization theory (Renard and de Marsily 1997). The problem of upscaling and derivation of effective properties has been treated extensively in the literature of various areas of research, and several reviews address the subject thoroughly (Renard and de Marsily 1997; Wen and Gomez Hernandez 1996; Neuman and Di Federico 2003; Sanchez-Vila et al. 2006).

In order to fix the ideas, we introduce first the length scales of the problem. Four characteristic lengths are involved: the size Δx of the fine grid cell, related to the geological model; an integral scale l_0 ("geological" correlation length) of the heterogeneity if possible to define; the size λ of the coarse grid cell chosen; and the overall size L of the full domain under study. In the case of a binary medium close to the percolation threshold, the information provided by l_0 might be advantageously replaced by that of the so-called "percolation" correlation length χ, which gives a measure of the size of finite clusters (Stauffer and Aharony 1992). In practical terms, the physically meaningful fine grid characteristic length scale comes up from a comparison between l_0 and Δx. The ratio of λ to l_0 (when it is possible to define the latter) or to Δx, in all other cases, it is frequently referred to as the "coarsening scale".

In terms of these characteristic scales, upscaling is the set of methods that allows one to transform accordingly properties given at a fine scale Δx into the corresponding ones at a coarse scale λ. In particular, the determination of a coarse scale hydraulic conductivity (K_{eff}) value is of special interest in various areas of research (K_{eff} may also be referred to as an effective or equivalent hydraulic conductivity, see Sanchez-Vila et al. (2006) for related nomenclature). The practical goal of upscaling is to achieve a coarse scale description in which the phenomenon under study (i.e. flow, transport) approximates as much as possible to that resulting of a fine scale description, while computational costs are expected to be greatly reduced. The task of accounting for important heterogeneity features such as connectivity while reducing spatial accuracy is crucial, especially in badly connected fracture patterns, or extremely heterogeneous media. One key concept related to this issue is the representative elementary volume (REV). Although the definition of the REV is often not formal and remains subjective, one could argue that if the REV linear size is smaller than λ, heterogeneity is smoothed out and upscaling does not present difficulties. If the REV size is greater than λ, heterogeneity fluctuations may compromise the ability to reproduce large-scale features. Regarding the REV and some cases of heterogeneity addressed in this article, Paleologos et al. (1996), considered that, for bounded heterogeneous media having lognormal K distribution and in the case of permeameter boundary conditions, the REV linear size should be at least eight times l_0, while, in the framework of the percolation theory, the REV size equals χ (which tends to infinity if the system is at the percolation threshold (Hunt and Ewing 2009)). Following this author, the composite correlation length of 3D media would be a product

Table 1 Length scales involved in upscaling and their description

Length scale	Description
Δx	Fine grid cell size (geological model scale)
l_0	Integral scale or "geological" correlation length[a]
λ	Coarse grid cell size (flow simulation scale)
χ	Percolation correlation length[b]
L	Size of the full domain in study
$\lambda/\Delta x$; λ/l_0	Coarsening scale[c,d]

[a] Paleologos et al. (1996)
[b] Hunt and Ewing (2009)
[c] Dykaar and Kitanidis (1992)
[d] Attinger (2003)

of a geological and percolation factors; this argument might also be pertinent for the REV (Table 1).

1.2 Objectives

While previous studies have addressed mainly the dependence of K_{eff} values with the coarsening scale (or at most its mean and variance), in the present study our aim is to study the scale dependence of the entire K_{eff} probability density functions (pdfs) and the statistics thereupon. The underlying idea is that if we are able to determine the pdf of K at the scale λ knowing both its pdf and correlation structure at the scale Δx, then the upscaling problem could be considered as being essentially solved (Nœtinger et al. 2005). This philosophy is very close to renormalisation group approaches developed lately (Attinger 2003).

Considering the scale dependance of the K_{eff} distributions rather than comparing a specific K_{eff} value obtained using one particular upscaling method in one particular media sample can be an advantageous approach, because two different upscaling techniques yielding the same distributions can be considered equivalent (in the sense of equivalent classes), even if for a particular media sample these techniques can provide different numerical values. As an example of this idea, and in the specific case of 2D isotropic lognormal distributions, the computation of K_{eff} for a media sample by using a finely gridded numerical simulation or by computing the geometric average of the actual K field (i.e. $K_{\text{eff}} = \left[\prod_{i=1}^{i=n} K_i\right]^{1/N}$) will yield the same distribution, even if numerical values may differ from one realization to another (Romeu and Nœtinger 1995).

In order to explore the potential of these ideas, we choose to follow a "numerical experimental approach". We consider two classical models for heterogeneous media: lognormal and binary media.

Lognormal fields have been extensively addressed in the literature since they were found to provide a good degree of approximation to field measurements of K (Hoeksema and Kitanidis 1985; Sudicky 1986). The K distribution within a single facies is frequently modelled as lognormally distributed by geostatisticians.

Binary or bimodal representations, as opposed to unimodal lognormal, came up as natural simplified models for media with two types of facies (or composites) or two characteristic values of K (sand-clay, sandstone-shale and fractured stone vs. non-fractured stone), being in this case the spatial organisation of the high-K facies frequently the key factor for determining effective properties. Interesting percolation effects can be expected in that situation in the case of different facies with high K contrasts. Combined models in which each facies possesses its own lognormal distributions have also been subject of study. In the context of the upscaling of naturally fractured reservoirs, de Dreuzy et al. (2001a, b p. 1, 2) considered random networks

of fractures having random apertures. In this case, spatial connectivity disorder is coupled with local (aperture) randomness. The obtained results provide an alternative interpretation framework.

In view of the strong dependence of K_{eff} on connectivity and thus on dimensionality (evident, for example, in the dimensionality dependence of the percolation thresholds and exponents) we chose to focus our work on 3D media despite the increase of computational cost involved and derived restrictions over the possible sizes of the samples to be studied.

The organisation of the article is as follows: we review existing results of upscaling of lognormal fields, before introducing upscaling of binary media, in which percolation theory and effective medium approaches are relevant. The retained numerical methodology is described: generation of the random media and numerical calculation of K_{eff}. The results for lognormal media are then presented and discussed, and compared with existing theories, with a partial conclusion where we discuss the conceptual implicances of our results. Binary media results are then framed in existing theoretical approaches and presented with focus on K_{eff} distributions and their statistics. We then present a final discussion and set the perspectives for future work.

1.3 Upscaling of Lognormal Fields

There is a vast amount of literature addressing the issue of upscaling lognormal media, the main reviews were mentioned in previous sections because lognormal media has been the test benchmark for upscaling by excellence. The theoretical approaches have a cornerstone on Matheron's work (Matheron 1967) that yielded exact results for lognormal isotropic stationary fields in 1D and 2D. An approximate expression is proposed in 3D that can be written as (Gutjahr et al. 1978):

$$K_{\text{eff}} = K_{\text{g}} \left[1 + \left(\frac{1}{2} - \frac{1}{D} \right) \sigma^2_{\ln K} \right] \tag{1.2.1}$$

where D is the euclidean dimension, K_{g} the geometric mean and $\sigma_0^2 \equiv \sigma^2_{\ln K}$.

Matheron conjetured that this result was actually the sum of the first two terms in the expansion of an exponential form:

$$K_{\text{eff}} = K_{\text{g}} \exp \left[\left(\frac{1}{2} - \frac{1}{D} \right) \sigma^2_{\ln K} \right] \tag{1.2.2}$$

The exponential conjecture is equivalent to the power average (Desbarats 1992):

$$K_{\text{eff}} = \left[\frac{1}{V} \int_V K^w \mathrm{d}V \right]^{1/w} \quad ; \quad w = \left(\frac{1}{2} - \frac{1}{D} \right) \tag{1.2.3}$$

Dagan (1993) demonstrated the validity of the conjecture using a series expansion up to the fourth order in the variance, but later De Wit (1995) and Abramovich and Indelman (1995) used sixth order perturbation methods to show that both Eqs. 1.2.2 and 1.2.3 are not strictly valid for $D = 3$, and that in the general case, the correct expression would need to include a small correction. This correction was shown to be structure dependent, it depends on the n-point statistics beyond the variance. This implies that any upscaling formula of the type of Eq. 1.2.3 is a priori incorrect. Nevertheless, power averaging is however widely used as a good approximation to K_{eff} (de Dreuzy et al. 2010).

Nœtinger (1994, 2000) argued by using renormalization methods that both expressions are valid for media with negligible correlation length, even if giving the latter a precise

mathematical sense remains a theoretical challenge. Stepanyants and Teodorovich (2003) found similar results using analogous methods. Paleologos et al. (1996) studied the case of a bounded domain having a lognormally distributed K, in the case of permeameter boundary conditions, and derived an explicit expression for K_{eff} that includes a domain integral which is a function of the integral scale. Note that every renormalization method is based upon some closure assumption that may be criticized in light of the known exact series expansion results presented above.

Lately, Attinger (2003) and Eberhard et al. (2004) used a coarse graining filtering technique combined with perturbation theory and renormalization group analysis to derive expressions for K_{eff} and its variance as a function of the coarsening scale.

Numerical simulations have also been extensively used to study upscaling of lognormal fields. Ababou et al. (1989) studied flow fields, head contours and K_{eff} in a single realization of a 3D lognormal random field.

Dykaar and Kitanidis (1992) employed a spectral decomposition approach in a bounded domain to obtain the values of K_{eff} and its variance as a function of the coarsening scale and compared these to different methods. Their results supported Matheron's conjecture.

Fenton and Griffiths (1993) used a MonteCarlo approach to study block conductivity in a 2D domain and found that its distribution was approximately lognormal.

1.4 Upscaling in Binary Media: Effective Medium Approaches, Connectivity and Percolation

Binary media has been studied often in the light of perturbation methods and effective medium theories (Maxwell 1873; Dagan 1989; Pozdniakov and Tsang 2004). Most of these methods are approximations that neglect detailed information about the spatial organisation of the facies or composite distribution (for example, connectivity). For example, Maxwell (1873) showed that for 3D spherical inclusions of a material 1 embedded in a material 2, K_{eff} is approximated by means of Eq. 1.3.1.

$$\left[\frac{K_{\text{eff}} - K_2}{K_{\text{eff}} + 2K_2}\right] = p_1 \left[\frac{K_1 - K_2}{K_1 + 2K_2}\right] \tag{1.3.1}$$

This expression is valid for a dilute regime (low volume fraction p_1 of composite 1). Later, Hashin and Shtrikman (1962) proved by means of variational principles that this expression equals the lower bound for K_{eff} if no other information than p_1 is provided, the upper may be obtained by interchanging labels 1 and 2 in Eq. (1.3.1). Later Dagan (1989) proposed a self consistent approximation valid also for lognormal distributions. In the following, p will refer to the volume fraction of the composite with higher K.

Connectivity has indeed been shown to be a very important feature in order to achieve accurate upscaled flow and transport properties, eventhough there is not a unified view of its quantitative characterization. Zinn and Harvey (2003) argued that "the full univariate distribution of conductivity values and the spatial covariance function for these values may not provide sufficient information to estimate effective flow and transport parameters". Other authors such as Knudby and Carrera (2005) agreed with this point of view, reviewing a set of statistical indicators of flow and transport connectivity suitable for different scenarios. As an example of the importance of connectivity characterization beyond two-point statistics, they use an example from Western et al. (2001) where two conductivity fields with practically same histogram and omnidirectional variograms (spatial covariance function) are evidently very different regarding connectivity which would imply strongly different effective properties. Knudby et al. (2006) showed that binary media with the same number, size and shape

of inclusions may not have the same effective properties due to the strong influence of the spatial organisation of the inclusions.

Percolation theory is intimately related to the issue of connectivity. Berkowitz and Balberg (1993) examined its applications to flow in porous media and also studied a system of permeable spheres with different K distributions studying its percolation exponents. Recently, Hunt and Ewing (2009) presented a comprehensive work regarding percolation theory and porous media.

The overall conductivity K of a system near the percolation threshold scales as:

$$K \propto (p - p_c)^{\mu} \tag{1.3.2}$$

where p_c is the critical value of p for which percolation transition occurs. Reported values for μ range from 1.88 to 2.09 (Hunt and Ewing 2009), however the coefficient of proportionality is not provided by percolation theory

The main differences between formal percolation systems and the situations motivating flow and transport simulations in realistic subsurface models may be summarize as following:

- The size of the sample is finite (this issue is addressed by finite size scaling within percolation theory, though the knowledge of universal non-singular functions is required for prediction) and may be statistically affected by unknown spatial correlations (Hunt and Ewing 2009). Spatial correlations are also known to change the percolation thresholds (Harter 2005; Guin and Ritzi Jr. 2008).
- The low-conducting K values are different from zero, and then there is an influence of the specific K_{high} and K_{low} values (this is for binary media, the situation for multiple facies media being still more complex).
- Percolation scaling applies mainly near the percolation threshold, and sometimes it's difficult to establish how far the system is from it (Berkowitz and Balberg 1993).

All these features tend to smear out the percolation transition, affecting the effective properties in a way that may be nontrivial to determine.

Moreover, connectivity and percolation properties in upscaling have been studied in models much more complex than binary media. For example, Fleckenstein and Fogg (2008) studied the relation between connectivity of high-K facies and average conductivity on five realizations of 3D geostatistical transition-probability based model, and showed how the connectivity of high K channels at different scales may influence the upscaling process. We consider however that the issue of upscaling and derivation of effective hydraulic conductivity K_{eff} in binary and lognormal media is far from being closed and still of huge interest.

2 Numerical Methodology

2.1 Description of the Upscaling Technique

Two main trends are followed regarding the implementation of numerical simulations for upscaling: local or global methods (for a more detailed and complete description we refer to Chen et al. (2003) and references therein). In local methods, a target block (coarse grid cell) is defined, and the fine grid K values of this block (plus a priori boundary conditions) are used to calculate K_{eff}. In the global ones (Bauer et al. 2008), basically flow is solved once over the entire domain and the region over which K_{eff} is calculated is then chosen. K_{eff} is then computed using a suitable post treatment of the flow field (pressure and local flow rate). This last method gives K_{eff} values that are expected to be less dependent on the

Table 2 Simulation parameters name, definitions and values for Sects. 3.1 and 3.2 (lognormal media)

Definition	Name	Section 3.1	Section 3.2
Fine grid mean of ln(K)	$\langle \ln(K) \rangle$	0	0
Fine grid variance of ln(K)	σ_0^2	1	0.5; 1; 2
Integral scale	l_0	$3\Delta x$	Δx
Coarsening scale	λ / l_0	$2^n/3$ ($n=2;3;4;5;6$)	2^n ($n=1;2;3;4$)
Refinement degree	r	1	5
Realizations per parameter set	n	5,000	5,000

particular upscaling conditions (for example, the choice of boundary conditions) used, but the computational cost is greater because it requires solving relatively larger linear systems.

In present study, we chose to employ a local upscaling technique with standard (permeameter) boundary conditions. More details about the technique are given in Sect. 2.3. Each coarse grid cell is an isotropic stationary realization of a lognormal or a binary random field, and is constituted by N^3 fine grid cells forming a simple cubic lattice. The fine grid cells have fixed linear size Δx. Over each coarse grid cell (of linear size $\lambda = N\Delta x$) K_{eff} is calculated as explained in Sect. 2.3.

2.2 Generation of Lognormal and Binary Media Samples

Several methods exist for generating realizations of random lognormal fields (turning bands (Tompson et al. 1989; Dietrich 1995), matrix decomposition (Davis 1987). In this study, we employed a FFT-based random field generator, FFTMA (Le Ravalec et al. 2000). The support dimensions and statistical parameters (type of distribution and variogram, geometric mean K_g, variance σ_0^2, integral scale l_0) may be adjusted for each realization.

The choice of parameters for the simulations in this first part has been made as following: Sect. 3.1: Standard normal distribution for ln(K): ($K_g = 1$ m/day ($\langle \ln(K) \rangle = 0$), variance $\sigma_0^2 = 1, l_0 = 3\Delta x$). Section 3.2: Same mean and integral scale values, the variance σ_0^2 was chosen to match that of the analytical derivations we compare our results to. Table 2 shows the simulation parameters name, definitions and values used in Sects. 3.1 and 3.2.

In the second part (binary media), first we generate a lognormal distribution (namely $f(K)$) with the same mean and variance than the ones used in the first part (Sect. 3). Then this lognormal distribution is binarized using a threshold value K_t to attribute to each fine grid cell a high-K or a low-K value (with $K_{\text{high}} = 100$ m/day and $K_{\text{low}} = 0.01$ m/day). Each fine grid cell having a value of $K_{i,j,k} < K_t$ has, after binarization, a value K_{low}, while each having a value of $K_{i,j,k} > K_t$ has then a value K_{high}. We recognize that other techniques could be followed, yielding to different high order correlation structures.

$$p = \frac{\int_{K_t}^{\infty} f(K)\,\mathrm{d}K}{\int_{-\infty}^{\infty} f(K)\,\mathrm{d}K} = 0.5\ erfc\left[-\frac{\ln(K_t) - \langle \ln(K) \rangle}{\left(2\sigma_0^2\right)^{1/2}}\right] \tag{2.1.1}$$

The volume fraction p is related to K_t by Eq. 2.1.1. The proportion p increases with decreasing K_t until the high-K fine grid gain connectivity (eventually reaching the percolation threshold). In this way, the connectivity of the high-K facies in the binarized medium is

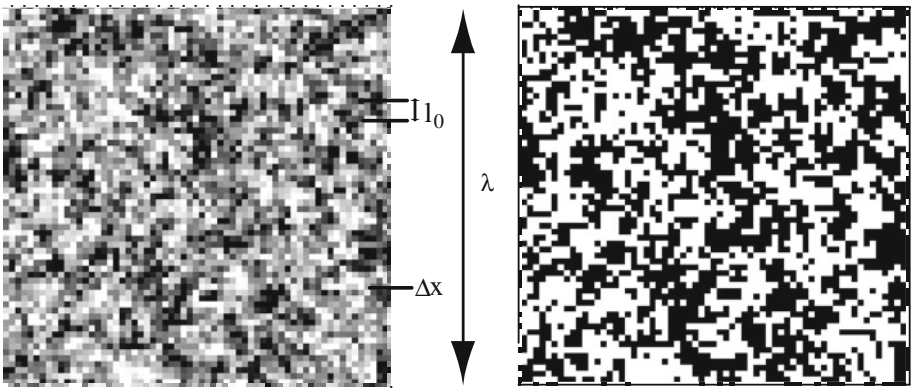

Fig. 1 *Grey* level maps: 2D cut of a 3D isotropic realization of a lognormal media sample (*left*) and of a binary media sample (*right*). The former corresponds to the media studied in Sect. 3, and is generated with parameters ($\langle \ln(K) \rangle = 0$), $\sigma_0^2 = 1$, $l_0 = 3\Delta x$ (*white* (*black*) colour: high (low) values of K). The latter represents the media studied in Sect. 4, the underlying lognormal realization having the same parameters, and the threshold value K_t is such that the high-K volume fraction p equals 0.5 (see Eq. 2.1.1); (*white*: K_{high}, *black*: K_{low}). The scales presented in Sect. 1.1 are indicated: one pixel in the image corresponds to one fine grid cell of linear size Δx; the integral scale l_0 (correlation length of the heterogeneity) equals $3\Delta x$ and, here as an example, $\lambda/\Delta x = 64$ (largest coarsening scale considered in this study)

controlled by varying l_0 in the underlying lognormal media. Figure 1 shows 2D cuts of the 3D lognormal and binary realizations where the length scales introduced in Sect. 1.1 are indicated.

The variance of the $\ln(K)$ in the binarized medium can be written as:

$$\sigma^2_{\ln K} = 4 \left(\ln(K_{\text{high}})\right)^2 p(1-p) \equiv \sigma^2_{\text{B}}(p) \tag{2.1.2}$$

This (fine grid) variance will be referred as σ^2_{B} and will be used to normalize the variance obtained at a given scale λ (coarse scale variance).

The choice of parameters in this second part has been made as following: Sect. 4.1: we address the limit to very large coarsening scale so this parameter is fixed and with the largest value considered in this study ($\lambda/\Delta x = 64$), we sample p densely in the region around p_c. The number of realizations is limited by the computational cost at this scale. Section 4.2: Our aim here is to study the pdf of the K_{eff} distribution, so we performed a large number of realizations and thus made the sampling of p less dense. Section 4.3: we sample p densely in the region around p_c, the diversity of coarsening scales implies a moderate computational cost and then a moderate number of realizations can be performed.

We used two different values of integral scale $l_0 = 3\Delta x$ (spatially correlated) and $l_0 = 0.1\Delta x$ (negligible correlation length). Table 3 shows the simulation parameters name, definitions and values used in Sects. 4.1, 4.2 and 4.3.

2.3 Numerical Calculation of K_{eff}

Because the realizations are in all cases isotropic, the calculation of K_{eff} is performed in the vertical direction (this is, we define $K_{\text{eff}} \cong K_{\text{eff zz}}$ hereafter).

For each coarse grid cell, no-flow (Neumann) condition is applied in the lateral sides (permeameter), and a constant head H_{in} (H_{out}) (Dirichlet) is applied in the top (bottom) side of the coarse grid cell. Following the nomenclature of Sanchez-Vila et al. (2006), this implies that the representative property calculated on the coarse grid cell is in truth a "pseudo-effective"

Table 3 Simulation parameters names, definitions and values for Sects. 4.1, 4.2 and 4.3 (binary media)

Definition	Name	Section 4.1	Section 4.2	Section 4.3
Fine grid mean of $\ln(K)$[a]	$\langle \ln(K) \rangle$	0	0	0
Fine grid variance of $\ln(K)$[a]	σ_0^2	1	1	1
Integral scale[a]	l_0	$0.1\,\Delta x; 3\Delta x$	$0.1\Delta x; 3\Delta x$	$0.1\Delta x; 3\Delta x$
Coarsening scale	$\lambda/\Delta x$	$2^6 = 64$	2^n $(n = 2;3;4;5;6)$	2^n $(n = 2;3;4;5)$
Refinement factor	r	1	1	1
High-K facies volume fraction	p	0 to 0.57 (dense sampling)	0.1 to 0.5 (loose sampling)	0.12 to 0.44 (dense sampling)
Realizations per parameter set	n	50	5,000	512

[a]Parameters of the underlying lognormal media (before binarization)

hydraulic conductivity (because it's dependent on the boundary conditions and not only on the medium considered). For the sake of simplicity, we will refer to this conductivity as K_{eff}.

The flow is then solved using a finite volume method where internodal transmissivities are calculated using the harmonic mean rule.

The linear system is solved using a biconjugate gradient stabilized method (BiCGSTAB) (Van der Vorst 1992) with ILU(0) preconditioning, and CSR storage. The iteration convergence tolerance was set to 10^{-9} m.

Once the flow is solved, K_{eff} is obtained as:

$$K_{\text{eff}} = \frac{Q}{(H_{\text{in}} - H_{\text{out}})} \tag{2.2.1}$$

Our simulation allows performing a refinement step (subgridding) of degree $r = \Delta x/\Delta x'$ after random field generation but before K_{eff} calculation in order to gain accuracy and reduce the bias error in the values of K_{eff} values caused by the 1D flow approximation which is implied in the finite volume method (Romeu and Nœtinger 1995). The use of this refinement step involves an important increase in the size of the system of linear equations to be solved for calculating K_{eff}. Because of this, it may be required to reduce the size of the domain in study in order to maintain the size of the linear system tractable. The refinement step is used when comparing to theoretical results in this article (Sect. 3.2). Finally, we emphasize that wherever the expression "$\ln(K)$" is shown in the results, we implicitly imply that the argument of the logarithm is divided by 1 m/day to make it dimensionless.

3 Lognormal Media: Results

The first part of this study concerns the issue of the pdf and statistics of K_{eff} distributions as a function of the coarsening scale for the lognormal stationary isotropic media.

3.1 Lognormality of the Upscaled Distributions:

The distribution of K_{eff} values for a particular medium depends a priori on its geometry and on the fine grid K values, but also on the upscaling method and conditions used (global or local upscaling, choice of boundary conditions, use of border regions (Wen et al. 2003), type of calculation of internodal transmissivities if using finite volumes) among other factors.

We observed that in our numerical experiments, for a wide range of coarsening scales, the distribution of $\ln(K_{\text{eff}})$ is well fitted by a normal (Gaussian) curve, as can be observed

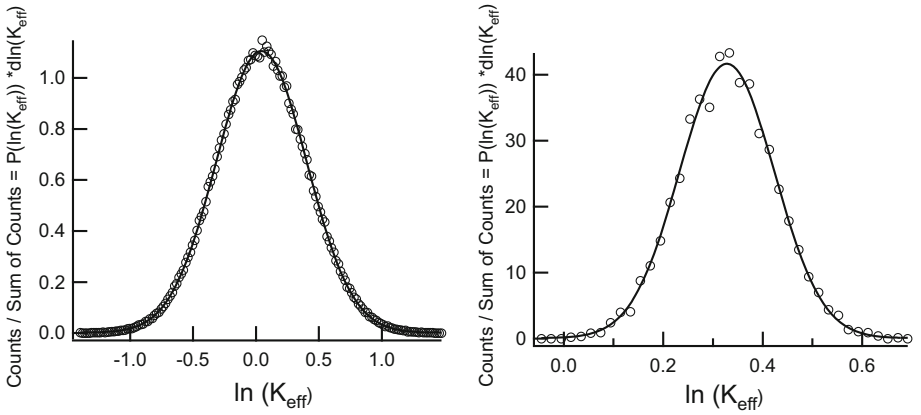

Fig. 2 Probability density function of $\ln(K_{\text{eff}})$ for small and large coarsening scales and their gaussian fit. *Left*: $\lambda/l_0 = 1.33(\lambda/\Delta x = 4)$. *Right* : $\lambda/l_0 = 21.33(\lambda/\Delta x = 64)$. This results correspond to 5,000 realizations with $l_0 = 3\Delta x$, $K_{\text{g}} = 1$ m/day, $\sigma_0^2 = 1$ and gaussian covariance. Histograms are performed following Scott's rule (Scott 1979) and then normalized in order to represent the probability distribution of $\ln(K_{\text{eff}})$

in Fig. 2. In this figure, we plot histograms of $\ln(K_{\text{eff}})$ distributions for typical small and large coarsening scales, and their lognormal datafit. Histograms are performed following Scott's rule (Scott 1979), particularly suitable for gaussian-like distributions. Results shown correspond to 5,000 realizations with $l_0 = 3\Delta x$, $K_{\text{g}} = 1$ m/day ($\langle \ln(K) \rangle = 0$), $\sigma_0^2 = 1$ and gaussian covariance. This result suggests that the lognormal distribution might represent a limit distribution for upscaling in given conditions. Two remarks can be done about this observation: on one hand, a previous work from Fenton and Griffiths (1993) obtained an analogous result in 2D, which would be consistent with Matheron's exact result in 2D (the log of geometric mean is additive in terms of logarithms). The extrapolation of this result to 3D is non-trivial. On the other hand, assuming that performing a field measurement implies the observation of an "effective property", this result would be consistent with the fact that these measurements have been reported to be well represented by lognormal distributions (Hoeksema and Kitanidis 1985; Sudicky 1986). Establishing overall extent and generality of the lognormal character of K_{eff} distributions is beyond the scope of the present study. Here, we use this observation as an hypothesis and we translate the study of the statistical properties to the variation of the mean and variance of $\ln(K_{\text{eff}})$ with the coarsening scale. Further discussion on this result will be presented in Sect. 3.3.

3.2 Variation of K_{eff} with the Coarsening Scale: Comparison with Theory

The numerical simulation described in previous sections is used to calculate the distribution of K_{eff} values at different coarsening scales. One practical criterion frequently used in flow simulations for establishing a target coarse grid size is to request the variance at the coarse scale to be a given fraction of the fine scale one. In this sense, the dependence of σ_λ^2 with λ for a simplified description of the heterogeneity, such as the ones we study in this study, may be a helpful "rule of thumb" for dealing with more complex descriptions.

Attinger (2003) and Eberhard et al. (2004) developed a coarse graining (filtering) technique that allows to derive the transition of K_{eff} between the arithmetic mean and the infinite

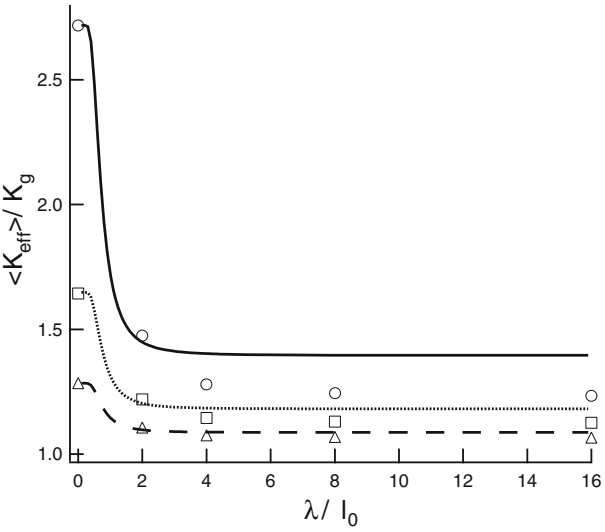

Fig. 3 *Symbols*: numerical results for $\langle K_{\text{eff}} \rangle / K_{\text{g}}$ as a function of λ / l_0 for $\sigma_0^2 = 0.5$ (*triangles*), $\sigma_0^2 = 1$ (*squares*) and $\sigma_0^2 = 2$ (*circles*). *Lines*: Analytical derivation of Eberhard et al. (2004) for the corresponding values of σ_0^2 ($a_s = 1$, $D = 3$)

3D medium value $K_{\text{g}} \exp(\sigma^2_{\ln K}/6)$ found by Matheron and others. It can be remarked that they used the assumption of scale invariance of lognormality for closure purposes.

In particular, they provided expressions for the variance σ_λ^2 at the coarse scale (to second order in perturbation theory) and K_{eff} (using renormalization group analysis to sum up higher orders) as a function of λ and l_0 (Eqs. (3.2.2) and (3.2.3)) where D is the number of dimensions, and $a_s \geq 1$ is a constant.

In order to make the comparison possible between the analytical expressions and our discrete numerical model, we transformed the variance defined at scale $\lambda / l_0 = 0$ (σ_f^2, analytical variance) to that defined at scale $\lambda / l_0 = 1$, (σ_0^2, numerical fine grid variance), using Eq. (3.2.3). This transformation factor is left as a function of a_s, then both $K_{\text{eff}}(\lambda / l_0)$ and $\sigma_\lambda^2(\lambda / l_0)$ were fitted simultaneously obtaining a best fit for $a_s = 1$.

Figures 3 and 4 show a comparison between the mean and variance of K_{eff} obtained numerically for three different values of σ_0^2 (5,000 realizations, $l_0 = \Delta x$, $K_{\text{g}} = 1$ m/day) and the fit with the analytical expression of Eberhard et al. (2004) ($D = 3$) for values of σ_f^2 so that the corresponding values of σ_f^2 match the former ones used in the simulations. For $a_s = 1$ and $D = 3$, the transformation factor between variances at scale $\lambda / l_0 = 1$ (σ_0^2) and scale $\lambda / l_0 = 0$ (σ_f^2) is given by $\sigma_0^2 = 0.31818\, \sigma_f^2$.

Both numerical model and analytical derivation assume a gaussian isotropic covariance. In this case, a refinement step of degree 5 ($r = 5$), introduced in Sect. 2.3, has been used in the numerical simulations to keep a reasonable accuracy in the calculation of K_{eff} (Romeu and Nœtinger 1995)

For $\sigma_\lambda^2(\lambda / l_0)$, numerical results are well fitted by the analytical expression and also one can observe that the normalized coarse grid variance $\sigma_\lambda^2(\lambda / l_0)/\sigma_f^2$ is independent of σ_f^2 (and then of σ_0^2), which is in accordance with the analytical prediction of Eq. (3.2.3).

For $K_{\text{eff}}(\lambda / l_0)$, the agreement is good for the smaller value of fine grid variance ($\sigma_0^2 = 0.5$) but the discrepancy increases as σ_0^2 increases and also as λ / l_0 increases. This may be due to bias effects on the calculation of K_{eff}, which are known to be more important as the variance increases (Romeu and Nœtinger 1995).

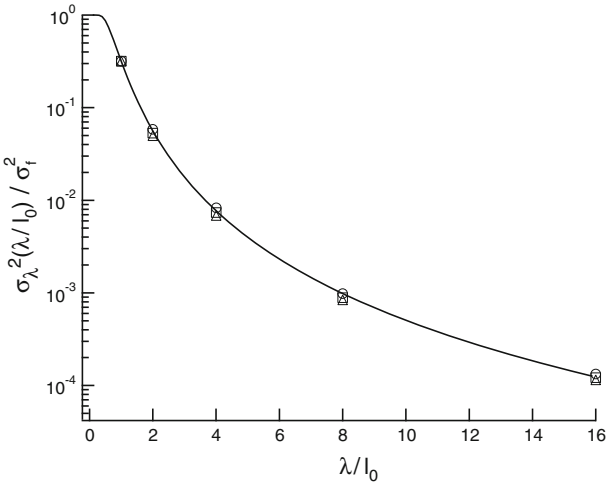

Fig. 4 *Symbols*: numerical results for the normalized coarse scale variance of $\ln(K_{\text{eff}})$, $\sigma_\lambda^2(\lambda/l_0)/\sigma_f^2$, as a function of λ/l_0 for $\sigma_0^2 = 0.5$ (*triangles*), $\sigma_0^2 = 1$ (*squares*) and $\sigma_0^2 = 2$ (*circles*). *Line*: Analytical derivation of Eberhard et al. (2004) for all variances

$$\langle K \rangle = K_{\text{g}} \exp\left(\frac{\sigma_f^2}{2}\right) \tag{3.2.1}$$

$$K_{\text{eff}}\left(\frac{\lambda}{l_0}\right) = \langle K \rangle \exp\left[-\frac{\sigma_f^2}{D} + \frac{\sigma_f^2}{D}\left(erf\left(\frac{l_0 a_s}{\sqrt{2}\lambda}\right)\right)^D\right] \tag{3.2.2}$$

$$\sigma_\lambda^2\left(\frac{\lambda}{l_0}\right) = K_{\text{g}}^2 \sigma_f^2 \left(erf\left(\frac{l_0 a_s}{\sqrt{2}\lambda}\right)\right)^D \tag{3.2.3}$$

Notice that for large values of λ, we have

$$\sigma_\lambda^2\left(\frac{\lambda}{l_0}\right) \approx \frac{2}{\sqrt{\pi}} K_{\text{g}}^2 \sigma_f^2 \left(\frac{l_0 a_s}{\sqrt{2}\lambda}\right)^D \tag{3.2.4}$$

The ratio $N = \left(\frac{\lambda}{l_0}\right)^D$ can be interpreted as the "number of independent heterogeneity units" contained in the coarse grid cell of size λ. Equation (3.2.3) appears then as a form of asymptotic variance reduction while increasing coarsening scale.

For the data shown in Fig. 4, we have used the following property:

$$\sigma_K^2 = K_{\text{g}}^2 \left\lfloor \exp\left(2\sigma_{\ln K}^2\right) - \exp\left(\sigma_{\ln K}^2\right) \right\rfloor \tag{3.2.4}$$

Which for order $O(\sigma_{\ln K}^2)$ becomes:

$$\sigma_K^2 = K_{\text{g}}^2\, \sigma_{\ln K}^2 = \sigma_{\ln K}^2 \quad (K_{\text{g}} = 1) \tag{3.2.5}$$

3.3 Partial Conclusions

In this section, we summarize the results for lognormal media. In Sect. 3.1, our results suggest a persistence of the lognormal character of the distributions through a wide range of

coarsening scales. The probability distributions of $\ln(K_{\text{eff}})$ obtained numerically over 5,000 realizations of lognormal samples are well fitted by a gaussian formula.

Our result is consistent with that of Fenton and Griffiths (1993) for 2D, and a theoretical foundation for this result could be sought on Matheron's result, that K_{eff} equals the geometric mean for lognormal fields in 2D (Matheron 1967). The idea is that in order to estimate K_{eff} for a coarse grid cell, we can replace the ensemble geometric mean by the following estimator:

$$K_{\text{eff}} = \left[\prod_{i=1}^{i=n} K_i\right]^{1/N} \tag{3.3.1}$$

This formula may capture the fine scale fluctuations. If it was exact, the emergence of the lognormality of K_{eff} distribution (or the normality of $\ln(K_{\text{eff}})$) would be directly related to the central limit theorem. This can be verified by taking logarithms to both sides of Eq. 3.3.1, the right side being then the sum of independent random values.
In the 3D case, even by means of a power law estimator (Nœtinger 1994, Eqs. 1.2.3), we cannot possibly make use of the central limit theorem to perform a similar argumentation. The lognormality of K_{eff} distribution could also be an artefact coming from the finite size of our statistical samples. In this order of idea, and in the particular context of upscaling through a power law formula, Jensen (1998) supports that in many situations power averages of lognormally distributed variables can be considered as being lognormally distributed. There is no evidence of mathematical argument to support this assumption, on the other hand it would be of extremely high computational cost to achieve a statistical sampling that allows one to distinguish between a lognormal distribution and other "close" distribution (in particular, in the cases of low variance). Our results can be interpreted within this context and limitations. We stress that our analysis did not consider two-point statistics at the coarse scale, so we cannot capture the spatial correlations at this scale.

Once under the hypothesis of the normality of $\ln(K_{\text{eff}})$, the mean and variance of its distribution were studied as a function of the coarsening scale. They are found to be in rather good agreement with analytical derivation of Attinger (2003) and Eberhard et al. (2004). Their prediction that the normalized coarse grid variance $\sigma^2_\lambda(\lambda/l_0)/\sigma^2_0$ does not depend on the fine grid variance σ^2_0 but only on the coarsening scale λ/l_0 is well reproduced by our results.

4 Binary Media: Results

In this section, we present results for simulations on binary media, focusing our attention on the variation of the K_{eff} distributions of and their statistics first as a function of p in the limit of very large λ, and then as a function of p and λ.

4.1 Limit to Very Large Coarsening Scale

We present here results for the largest coarsening scale studied ($\lambda/\Delta x = 64$) which is an approximation to the infinite coarse grid cell K_{eff} value.

In this limit, the media under study is analogous to a percolation network. The underlying lognormal distribution has $K_g = 1$ m/day ($\langle \ln(K) \rangle = 0$), $\sigma^2_0 = 1$ and gaussian isotropic covariance, and $l_0 = 0.1\Delta x$ (negligible correlation length) or $l_0 = 3\Delta x$ (correlated medium). The variance of the binarized distribution at the fine scale (used to normalize in the figures) is given by Eq. 2.1.2.

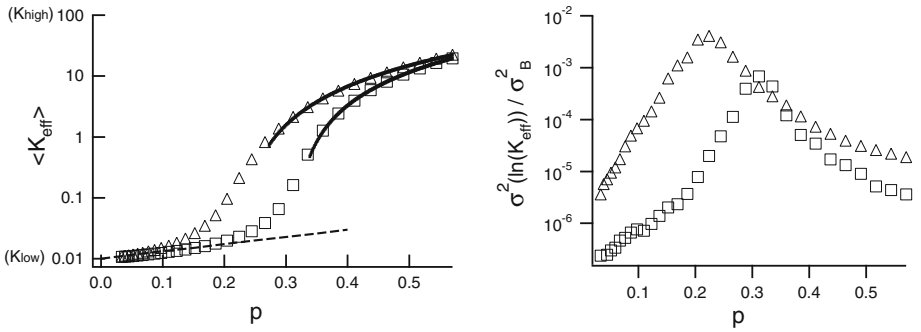

Fig. 5 Mean of K_{eff} (*left*) and normalized variance of $\ln(K_{\text{eff}})$ (*right*) as a function of p for $\lambda/\Delta x = 64$ (largest coarsening scale) and $l_0 = 0.1\Delta x$ (*squares*) or $l_0 = 3\Delta x$ (*triangles*). Data shown corresponds to 50 realizations for each p value. The normalized variance displays a peak at the percolation threshold p_c, which value is lower for the correlated case. *Dashed line*: Maxwell's approximation (given by Eq. (1.3.1) and valid for low p). *Full line*: Data fit with expression of Eq. (1.3.2) for $p > p_c$ using $p_c = 0.22(l_0 = 3\Delta x)$ and $p_c = 0.31(l_0 = 0.1\Delta x)$, yielding $\mu = 1.96 \pm 0.1$ and 1.68 ± 0.1 respectively. The values of p_c used to fit correspond to the maximum of the normalized variance

Figure 5 shows the variation of the mean and normalized variance of the distribution of K_{eff} (actually of $\ln(K_{\text{eff}})$ for the normalized variance, for easier visualization) as a function of p for $\lambda/\Delta x = 64$. The normalized variance is bell shaped and has a peak at p_c. The peak at $p = 0.31$ for the negligible correlation case ($l_0 = 0.1\Delta x$) is in agreement with the theoretical value for site percolation in a simple cubic lattice ($p_c = 0.311$).

As l_0 increases to $3\Delta x$ (and the connectivity of the high-K fine grid cells increases), p_c decreases to 0.22 (this value is taken from the maximum of the normalized variance). This type of behaviour has already been observed by other authors (Harter 2005; Guin and Ritzi Jr. 2008). Also as l_0 increases the percolation transition is smeared out over a more extended range of p. This can be interpreted in terms of the finite size scaling, with spatial correlations making the sample smaller in a statistical sense (Hunt and Ewing 2009). This idea has its counterpart for lognormal media in Eq. 3.2.4 and therein.

In the figure, one can observe that Maxwell's approximation (Eq. 1.3.1) is in good agreement with our numerical results up to $p \sim 0.2$ (this approximation is indeed valid for dilute regime or non-overlapping inclusions (Pozdniakov and Tsang 2004). At this value, the normalized variance displays a marked change of slope which may be due to the fact that high conductivity cells gain connectivity beginning the onset of percolation, with the dilute regime is no longer valid. On the other hand, above the percolation threshold, the percolation exponents provided by the data fit ($\mu = 1.96 \pm 0.1$ for a correlated medium and 1.68 ± 0.1 for negligible correlation length) are in acceptable accordance with the possible values reported by Hunt and Ewing (2009), ranging from 1.88 to 2.09.

4.2 K_{eff} Distributions: Dependence with Coarsening Scale

We will now address the issue of the dependence of the K_{eff} pdf with the coarsening scale. When the coarse grid cell size equals the fine one, each cell has a value equal to K_{low} or K_{high}. In the limit of very large coarse grid cell, the distribution of K_{eff} yields a well-defined K_{eff} value studied in the previous section. A clear picture of intermediate situation, which depends strongly on the connectivity properties, is crucial for determining the REV size and avoiding difficulties in any upscaling procedure.

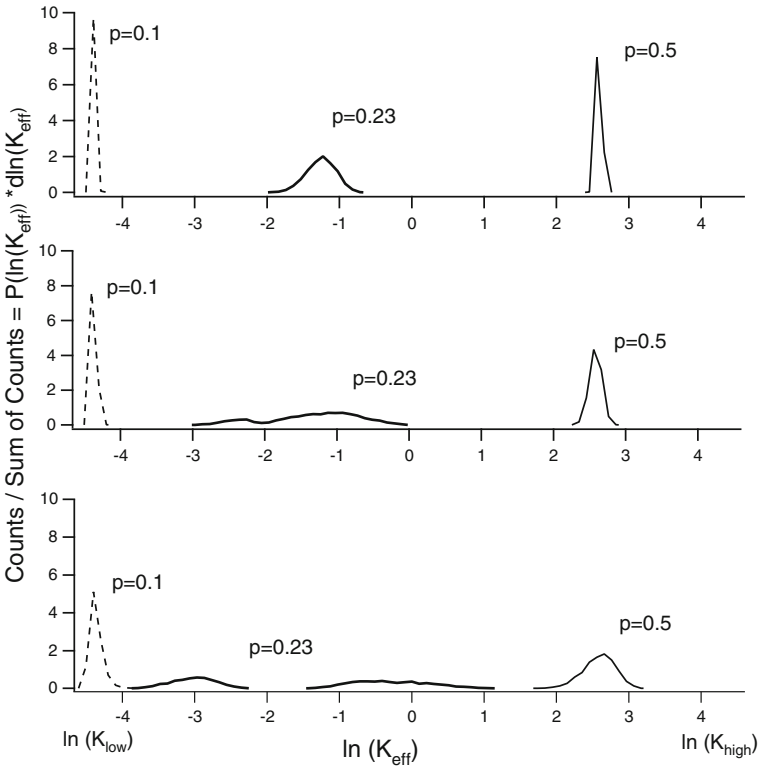

Fig. 6 Probability density function of $\ln(K_{\text{eff}})$ for 5,000 realizations for $\lambda/\Delta x = 64$ (*top*), $\lambda/\Delta x = 32$ (*center*), $\lambda/\Delta x = 16$ (*bottom*) ($l_0 = 3\Delta x$). *Dashed line* $p = 0.1$; *full thick line*: $p = 0.23$; *full thin line*: $p = 0.5$. The behaviour of the distribution of $\ln(K_{\text{eff}})$ for $p = 0.23$ shows that near $p_c (p = 0.22)$ a well-defined K_{eff} value may be reached only approaching $\lambda/\Delta x = 64$. This behaviour may have strong consequences in the REV determination process

In Fig. 6, we depict this situation by showing histograms for three values of coarsening scales and three values of p (the intermediate one close to p_c) for the case $l_0 = 3\Delta x$ (the case $l_0 = 0.1\Delta x$ is rather similar as much as concerns the particular analysis we perform in this section, but evidently p_c is different).

For the largest coarsening scale ($\lambda/\Delta x = 64$, top) the scenario is that presented in Sect. 4.1: the values of K_{eff} are well defined for each distribution for all the values of p, and the mean and variance of the distribution is basically given by the results shown in Fig. 5. For the two p values far from p_c, K_{eff} approximates K_{low} or K_{high}, respectively.

As $\lambda/\Delta x$ decreases, the distribution for p near p_c splits beginning a transition towards the fine scale bivaluated distribution where K_{eff} is not well defined and the variance increases markedly, while for p far from p_c there is still a well-defined K_{eff} value (the variance however increases moderately).

The results shown in Fig. 6 suggests that, close to $p_{\mathbf{c}}$, the possibility of defining a REV by means of a well-defined and representative K_{eff} value may be reached only for $\lambda/\Delta x = 64$. At this scale, both distributions far and near p_c are well fitted by a Gaussian function.

Figure 7 shows quantitatively how the decrease of the normalized variance with $\lambda/\Delta x$ is remarkably slower at p near p_c. Media in this condition will then frequently present as high degree of difficulty for upscaling procedures.

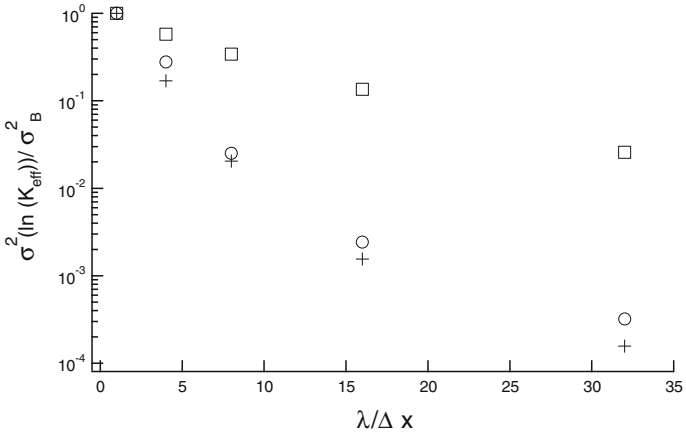

Fig. 7 Normalized variance of $\ln(K_{\text{eff}})$ for 5,000 realizations of a binary media sample having $p = 0.1$ (*plus sign*); 0.23 (*squares*); 0.5(*circles*), as a function of $\lambda/\Delta x (l_0 = 3\Delta x)$. As the p values approaches the percolation threshold ($p_c \sim 0.22$) the decrease of the normalized variance with $\lambda/\Delta x$ becomes remarkably slow comparing to when p is far from p_c

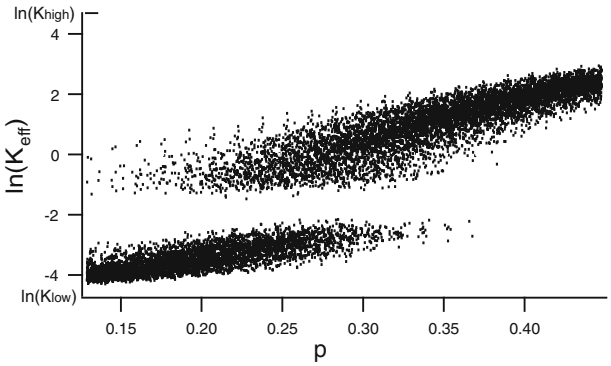

Fig. 8 Scatter plot of $\ln(K_{\text{eff}})$ for $\lambda/\Delta x = 16$ and $l_0 = 3\Delta x$. The data shown corresponds to 512 realizations for each of 21 values of p ranging from 0.13 to 0.45. It can be observed that there is a range or gap of extreme low probability ($\ln(K_{\text{eff}}) \sim -2$). Its width decreases as $\lambda/\Delta x$ increases

4.3 Statistics of K_{eff} Distributions

We address here the statistics of K_{eff} distributions with a dense sampling in p. Figure 8 shows a scatter plot of K_{eff} values that depicts the percolation transition at an intermediate coarsening scale ($\lambda/\Delta x = 16$). One can observe at this coarsening scale the range of K_{eff} values with extreme low probability ($\ln(K_{\text{eff}}) \sim -2$). The width of this range increases as $\lambda/\Delta x$ decreases. From distributions such as shown in Fig. 8, we have computed the mean (Fig. 9) and the normalized variance (Fig. 10). In Fig. 9, one can observe that for $l_0 = 3\Delta x$ and $l_0 = 0.1\ \Delta x$, as $\lambda/\Delta x$ increases, the curves tend towards that corresponding to the very large coarsening scale limit.

In Sect. 4.1, it has been shown that, in this limit an increase of spatial correlation (and the increase of high-K connectivity involved) have two effects: changing p_c and smearing out the percolation transition over a more extended range of p. On the other hand, it is

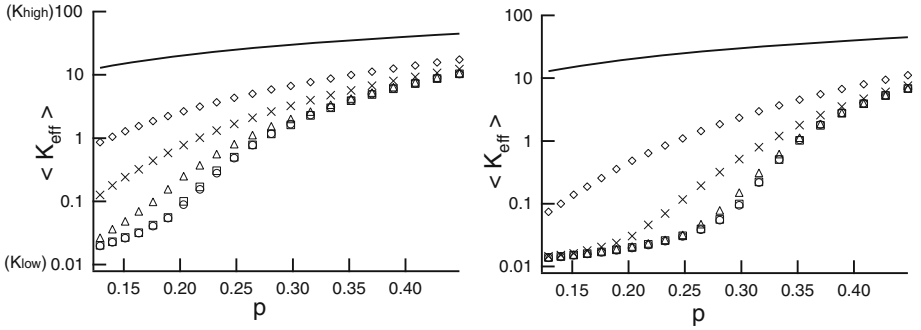

Fig. 9 Mean of K_{eff} over 512 realizations performed for each of 21 different p values for $\lambda/\Delta x = 64$ (*circles*), $\lambda/\Delta x = 32$ (*squares*), $\lambda/\Delta x = 16$ (*triangles*), $\lambda/\Delta x = 8$ (*crosses*), $\lambda/\Delta x = 4$ (*diamonds*). *Full line*: Mean of fine grid K values (limit for $\lambda/\Delta x = 1$). *Left*: $l_0 = 3\Delta x$, *right*: $l_0 = 0.1\Delta x$. The curves tend asymptotically towards that corresponding to the very large coarsening scale limit

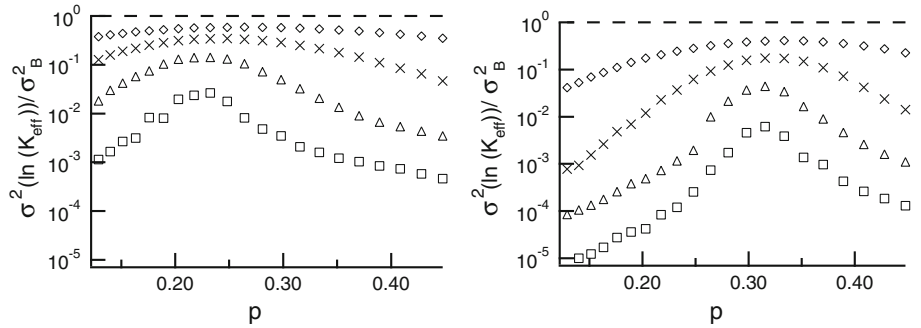

Fig. 10 Normalized variance of $\ln(K_{\text{eff}})$ obtained from 512 realizations performed for each of 21 different p values (each curve corresponds to a $\ln(K_{\text{eff}})$ distribution such as the one shown in Fig. 7). *Left*: $l_0 = 3\Delta x$, *right*: $l_0 = 0.1\Delta x$. *Squares*: $\lambda/\Delta x = 32$; *triangles*: $\lambda/\Delta x = 16$; *crosses*: $\lambda/\Delta x = 8$; *diamonds*: $\lambda/\Delta x = 4$; *dashed line*: analytical value for $\lambda/\Delta x = 1$

known from finite size scaling that reducing the sample size (i.e. $\lambda/\Delta x$) may also generate the latter. Figure 9 shows how this effect varies with the coarsening scale with respect to the mean of the distributions. The coincidence between, for example, crosses in Fig. 8 left ($\lambda/\Delta x = 8$; $l_0 = 3\Delta x$), and diamonds in Fig. 9 right ($\lambda/\Delta x = 4$; $l_0 = 0.1\ \Delta x$), may suggest the difficulty to distinguish, in terms of K_{eff} statistics, an increase in l_0 from a decrease in $\lambda/\Delta x$.

However these two can be clearly distinguished if analysing the normalized variance (Fig. 10). This is because due to the change of p_c, the position of the normalized variance maximum is shifted. Moreover, the value of this maximum may seem to be independent of the coarsening scale for $l_0 = 0.1\ \Delta x$, while for the case $l_0 = 3\ \Delta x$ it seems to drift to high p values as $\lambda/\Delta x$ decreases.

5 Summary, Discussion and Conclusions

The results presented in previous sections depict the upscaling scenario for two classical models of heterogeneous media: lognormal and binary media.

For lognormal media, the apparent lognormality of K_{eff} distributions at all scales considered suggests that this type of distribution may behave as a limit distribution (for given upscaling conditions). Despite the fact that there is no theoretical evidence that supports this hypothesis in 3D (for 2D an argumentation is proposed in Sect. 3.3), it would be consistent with previous results in 2D (Fenton and Griffiths 1993) and also with the lognormal character of field measurements (as discussed in detail in Sect. 3.1). The emergence of such "stable" distributions under successive up scaling steps would be a deep property, close to renormalization group philosophy. Under this assumption, we focused on the parameters characterizing this distribution, in particular the mean and variance, as a function of the coarsening scale. The decrease of these two with increasing coarsening scale has been derived analytically in previous studies (see references in Sect. 3.2). The mean and variance of the K_{eff} distributions obtained in our simulations are in rather good agreement with these analytical results, in particular, with the fact that the normalized coarse grid variance $\sigma_\lambda^2(\lambda/l_0)/\sigma_0^2$ does not depend on the fine grid variance σ_0^2 but only on the coarsening scale λ/l_0.

Next, we considered binary media with two characteristic K values with a given volume fraction p of high-K facies (binary or bimodal, as opposed to a unimodal lognormal distribution characterized only by a given mean and variance). In this case, the connectivity of the high-K facies is known to be crucial. As our binary samples are constructed by binarizing lognormal samples, we were able to modify the connectivity of the former ones by varying the integral scale l_0 of the latter ones.

In the limit of a very large coarsening scale, we show that when l_0 increases (i.e. the connectivity is increased), p_c decreases and also the percolation transition is smeared out over a more extended range of p, as reported by other authors. We must recall that the finite value of $K_{\text{high}}/K_{\text{low}}$ (as opposed to the infinite value of classical percolation systems) used in our simulations may also contribute to this smearing out; in this study, we do not investigate the influence and relative weight of this contribution.

At this scale, the K_{eff} distributions have well-defined K_{eff} value independently of the value of p, then as $\lambda/\Delta x$ decreases, the behaviour is different: near p_c the distribution splits and extends over a wide range of K_{eff} values, far from p_c they increase their width and keep a well-defined K_{eff} value that tends slowly to either K_{low} or K_{high}. The remarkably slow rate of decrease of the normalized variance with $\lambda/\Delta x$ near p_c describes quantitatively the degree of difficulty that this situation may pose for upscaling (compared to p far from p_c).

Finally, we compare the results for the two types of media studied. The normalized variance in the lognormal case decreases approximately by a factor of 10^2 at scale $\lambda/l_0 = 8$ (with respect to $\lambda/l_0 = 1$) and of 10^3 at scale $\lambda/l_0 = 16$. These values are of the same order than the corresponding ones for binary media when p is far from p_c, but differ strongly when p is near p_c, in which case the decrease factor is of order 10^0 for $\lambda/\Delta x = 8$ and of order 10^1 for $\lambda/\Delta x = 16$ (there is a difference of order 10^2 for both scales). This result implies a similar degree of difficulty for upscaling procedures in lognormal media and binary media with p far from p_c, both cases being markedly less difficult than the case of binary media with p near p_c.

6 Perspectives

On the theoretical side, justifying the apparent emergence of a limit distribution of the hydraulic conductivity at a given scale remains challenging.

Matheron's exact result for lognormal fields in 2D (that K_{eff} equals the geometric mean) suggests a proof for this case, by means of the central limit theorem, even if the result of

Matheron involves the geometric mean in an averaged sense and not for specific realizations. In the 3D case such an argument will not work even using a power mean of arbitrary exponent (this exponent is estimated to have a value equal to 1/3 for 3D (Nœtinger 1994)). A first approach could be inversing the problem and finding which types of distributions are stable under a power mean average. More generally, previous studies of K_{eff} of 2D Discrete Fracture Networks (DFNs) in which random conductivities are superimposed to an existing geometric disorder (the DFN random geometry) exhibit the emergence of such apparent lognormal distributions (Charlaix et al. 1987; de Dreuzy et al. 2001a, b,2002). In addition, such media exhibits also the emergence of power law averages with varying exponents that depends on the connectivity of the underlying DFN, even in 3D cases (de Dreuzy et al. 2010). Nœtinger and Jarrige (2012) also developed a method allowing to test such results on 3D DFN involving random fractures. In the same spirit, in close analogy with the already known percolation scaling laws valid for p near p_c, we could also anticipate the emergence of a non-trivial universal stable law for K_{eff} distributions for systems with p near p_c. Finding such limiting distributions will probably be of major importance in order to get a better understanding of the REV variation and determination. It would also be interesting to study the two-point statistics dependence on the coarsening scale and on the multipoint structure of the fine scale description. Even though a systematic and intensive numerical study of these features would require an enormous amount of computational resources due to the size of the statistical sampling required, this would be essential in order to anticipate which are the main features that must be kept throughout the upscaling workflow. A compromise must be found between numerical accuracy, size of the averaging volume, fine scale variance and correlation length. Typically, the case of media having a small correlation length (with respect to a reference length) and a very large variance σ_0^2 such that the product $\sigma_0^2\ (l_0)^{\text{D}}$ remains fixed seems of interest.

For more practical purposes, treating models with more than two facies remains essential. The description of a medium with a number of geological facies each one carrying a different K distribution is of current practice. The possible generalization of the results obtained in this study for binary media using suitable lumping procedures seems of interest.

Finally, we discuss the possible future applications of the present study. One is related to multiscale history matching techniques, in which dynamic information is added from coarse scale to the fine one (Nœtinger et al. 2005). The main idea is to use the resulting K_{eff} distributions in order to propose a suitable parameterization of the matching problem. The main idea is to generate these distributions at the coarse scale, even if the associated numerical simulations can still be performed at the fine scale for accuracy purposes. This can be done in zones close to injection or production wells. This is equivalent to decouple the parameterization of the geological model and the one associated with the flow simulation. As a prerequisite, developing such techniques would require at least to know the two-point structure at the coarse scale. As a first guess, one could use the K_{eff} pdf as computed in this study, while keeping the fine scale two-point structure properly renormalized. Such an approach seems to be reasonable in the lognormal case. Its applicability to binary media with p near p_c seems more uncertain. This is an interesting issue, closely related to REV determination problem.

References

Ababou, R., McLaughlin, D.B., Gelhar, L.W., Tompson, A.F.B.: Numerical imulation of three-dimensional saturated flow in randomly heterogeneous porous media. Transp. Porous Media **4**, 549–565 (1989)

Abramovich, B., Indelman, P.: Effective permittivity of log-normal isotropic random-media. J. Phys. A **28**, 670–693 (1995)
Attinger, S.: Generalized coarse graining procedures for flow in porous media. Comput. Geosci. **7**, 253–257 (2003)
Bauer, D., Talon, L., Ehrlacher, A.: Computation of the equivalent macroscopic permeability tensor of discrete networks with heterogeneous segment length. ASCE J. Hydraul. Eng. **6**, 784–793 (2008)
Berkowitz, B., Balberg, I.: Percolation theory and its application to groundwater hydrology. Water Resour. Res. **29**(4), 775–794 (1993)
Charlaix, E., Guyon, E., Roux, S.: Permeability of a random array of fractures of widely varying apertures. Transp. Porous Media **2**, 31–43 (1987)
Chen, Y., Durlofsky, L.J., Gerritsen, M., Wen, X.H.: A coupled local-global upscaling approach for simulating flow in highly heterogeneous formations. Adv. Water Resour. **26**, 1041–1060 (2003)
Dagan, G.: Flow and Transport in Porous Formations. Springer-Verlag, New York (1989)
Dagan, G.: Higher correction of effective permeability of heterogeneous isotropic formations of lognormal conductivity distribution. Transp. Porous Media **12**, 279–290 (1993)
Davis, M.: Production of conditional simulation via the lu triangular decomposition of the covariance matrix. Math. Geol. **19**(2), 99–107 (1987)
de Dreuzy, J.-R., Davy, P., Bour, O.: Hydraulic properties of two-dimensional random fracture networks following power law distributions of length and aperture, 1 effective connectivity. Water Resour. Res. **37**(8), 2065–2078 (2001)
de Dreuzy, J.-R., Davy, P., Bour, O.: Hydraulic properties of two-dimensional random fracture networks following a power law length distribution: 2. Permeability of networks based on lognormal distribution of apertures. Water Resour. Res. **37**(8), 2079–2095 (2001)
de Dreuzy, J.-R., Davy, P., Bour, O.: Hydraulic properties of two-dimensional random fracture networks following power law distributions of length and aperture. Water Resour. Res. **38**(12), 1276–1284 (2002)
de Dreuzy, J.-R., de Boiry, P., Pichot, G., Davy, P.: Use of power averaging for quantifying the influence of structure organization on permeability upscaling in on-lattice networks under mean parallel flow. Water Resour. Res. **46**, W08519 (2010)
De Wit, A.: Correlation structure dependence of the effective permeability of heterogeneous porous media. Phys. Fluids **7**, 2553–2562 (1995)
Desbarats, A.J.: Spatial averaging of hydraulic conductivity in three-dimensional heterogeneous porous media. Math. Geol. **24**(3), 249–267 (1992)
Dietrich, C.R.: A simple and efficient space domain implementation of the turning bands method. Water Resour. Res. **31**(1), 147–156 (1995)
Dykaar, B.B., Kitanidis, P.K.: Determination of the effective hydraulic conductivity for heterogeneous porous media using a numerical spectral approach: 2. Results. Water Resour. Res. **28**(4), 1167–1178 (1992)
Eberhard, S. Attinger, Wittum, G.: Coarse graining for upscaling of flow in heterogeneous porous media. Multiscale Model. Simul. **2**, 269 (2004)
Fenton, G.A., Griffiths, D.V.: Statistics of block conductivity through a simple bounded stochastic medium. Water Resour. Res. **26**(6), 1825–1830 (1992)
Fleckenstein, J.H., Fogg, G.E.: Efficient upscaling of hydraulic conductivity in heterogeneous alluvial aquifers. Hydrogeol. J. **16**, 1239–1250 (2008)
Guin, A., Ritzi, R.W. Jr..: Studying the effect of correlation and finite-domain size on spatial continuity of permeable sediments. Geophys. Res. Lett. **35**, L10402 (2008)
Gutjahr, A.L., Gelhar, L.W., Bakr, A.A., McMillan, J.R.: Stochastic analysis of spatial variability in subsurface flow 2: Evaluation and application. Water Resour. Res. **14**, 953–959 (1978)
Harter, T.: Finite-size scaling analysis of percolation in three-dimensional correlated binary Markov chain random fields. Phys. Rev. E **72**(2), 26120 (2005)
Hashin, Z., Shtrikman, A.: Variational approach to the theory of the effective magnetic permeability of multiphase materials. J. Appl. Phys. **33**, 3125–3131 (1962)
Hoeksema, R.J., Kitanidis, P.K.: Analysis of spatial variability of properties of selected aquifers. Water Resour. Res. **21**(4), 563–572 (1985)
Hunt, A.G., Ewing, R.: Percolation Theory for Flow in Porous Media, Lecture Notes in Physics, vol. 771, 2nd edn. Springer (2009)
Jensen, J.L.: Some statistical properties of power averages for lognormal samples. Water Resour. Res. **34**(9), 2415–2418 (1998). doi:10.1029/98WR01557
Journel, A.G., Deutsch, C.V., Desbarats, A.J.: Power averaging for block effective permeability. Paper presented at 56th California Regional Meeting, SPE, Oakland, California (1986)
Knudby, C., Carrera, J.: On the relationship between indicators of geostatistical, flow and transport connectivity. Adv. Water Resour. **28**, 405–421 (2005)

Knudby, C., Carrera, J., Bumgardner, J.D., Fogg, G.E.: Binary upscaling-the role of connectivity and a new formula. Adv. Water Resour. **29**, 590–604 (2006)
Landau, L.D., Lifshitz, E.M.: Electrodynamics of Continuous Media. Pergamon, Tarrytown (1960)
Le Ravalec, M., Nœtinger, B., Hu, L.Y.: The FFT moving average (FFT-MA) method: an efficient tool for generating and conditioning Gaussian simulations. Math. Geol. **32**(6), 701–723 (1995)
Matheron, G.: Eléments pour une Théorie des Milieux Poreux. Masson, Paris (1967)
Maxwell, J.C.: Electricity and Magnetism, 1st ed. Clarendon, Oxford (1873)
Neuman, S.P., Di Federico, V.: Multifaceted nature of hydrogeologic scaling and its interpretation. Rev. Geophys. **41**(3), 1014 (2003)
Nœtinger, B.: The effective permeability of an heterogeneous porous medium. Transp. Porous Media **15**, 99–127 (1994)
Nœtinger, B.: Computing the effective permeability of log-normal permeability fields using renormalization methods. C.R. Acad. Sci. Sci Terre Des Planètes **331**, 353–357 (2000)
Nœtinger, B., Jarrige, N.: A quasi steady state method for solving transient Darcy flow in complex 3D fractured networks. J. Comput. Phys. **231**(1), 23–38 (2012)
Nœtinger, B., Artus, V., Zargar, G.: The future of stochastic and upscaling methods in hydrogeology. Solicitated Review Paper of Hydrogeol. J. **13**, 184–201 (2005)
Paleologos, E.K., Neuman, S.P., Tartakovsky, D.: Effective hydraulic conductivity of bounded, strongly heterogeneous porous media. Water Resour. Res. **32**(5), 1333–1341 (1996)
Pozdniakov, S., Tsang, C.-F.: A self-consistent approach for calculating the effective hydraulic conductivity of a binary, heterogeneous medium. Water Resour. Res. **40**, W05105 (2004)
Renard, P, de Marsily, G.: Calculating equivalent permeability: a review. Adv. Water Resour. **20**(5–6), 253–278 (1997)
Romeu, R.K., Nœtinger, B.: Calculation of internodal transmissivities in finite difference models of flow in heterogeneous porous media. Water Resour. Res. **31**(4), 943–959 (1995)
Sanchez-Vila, X., Guadagnini, A., Carrera, J.: Representative hydraulic conductivities in saturated groundwater flow. Rev. Geophys. **44**, RG3002 (2006)
Scott, D.W.: On optimal and data-based histograms. Biometrika **66**(3), 605–610 (1979)
Stauffer, D., Aharony, A.: Introduction to Percolation Theory. Taylor and Francis, London (1992); revised 2nd edition (1994)
Stepanyants, Y.A., Teodorovich, E.V.: Effective hydraulic conductivity of a randomly heterogeneous porous medium. Water Resour. Res. **39**(3), 1065 (2003)
Sudicky, E.A.: A natural gradient experiment on solute transport in a sand aquifer: Spatial variability of hydraulic conductivity and its role in the dispersion process. Water Resour. Res. **22**, 2069–2082 (1986)
Tompson, A.F.B., Ababou, R., Gelhar, L.W.: Implementation of the three-dimensional turning bands random field generator. Water Resour. Res. **25**(10), 2227–2243 (1989)
Vander Vorst, H.A.: Bi-CGSTAB: a fast and smoothly converging variant of Bi-CG for the solution of nonsymmetric linear systems. SIAM J. Scientific Stat. Comput. **13**, 631–644 (1992)
Western, A.W., Blöschl, G., Grayson, R.B.: Towards capturing hydrologically significant connectivity in spatial patterns. Water Resour. Res. **37**(1), 83–97 (2001)
Wen, X.H., Gomez Hernandez, J.J.: Upscaling hydraulic conductivities in heterogeneous media: an overview. J. Hydrol. **183**(1–2), 9–32 (1996)
Wen, X.H., Durlofsky, L.J., Edwards, M.G.: Use of border regions for improved permeability upscaling. Math. Geol. **35**, 521–547 (2003)
Zinn, B., Harvey, C.F.: When good statistical models of aquifer heterogeneity go bad: A comparison of flow, dispersion and mass transfer in multigaussian and connected conductivity fields. Water Resour. Res. **39**(3), 1051 (2003)